

Signal characteristics of surface seismic explosive sources near the West Antarctic Ice Sheet divide

Marianne S. KARPLUS,^{1*} Nori NAKATA,² Galen KAIP,¹ Steven H. HARDER,¹ Lucia F. GONZALEZ,¹ Adam D. BOOTH,³ Emma C. SMITH,³ Stephen A. VEITCH,^{1,4} Jacob I. WALTER,⁵ Poul CHRISTOFFERSEN,^{6,7}

¹*Dept. of Earth, Environmental, and Resources Sciences, University of Texas at El Paso, El Paso, TX*

²*Earth, Atmospheric, and Planetary Sciences, Massachusetts Institute of Technology, Cambridge, MA*

³*School of Earth and Environment, University of Leeds, Leeds, UK*

⁴*Earthscope Consortium, Socorro, NM*

⁵*School of Geosciences, University of Oklahoma, Norman, OK*

⁶*Institute for Marine and Antarctic Studies, University of Tasmania, Hobart, Tasmania*

⁷*Australian Centre for Excellence in Antarctic Science*

Correspondence: Marianne Karplus <mkarplus@utep.edu>

ABSTRACT. Seismic imaging in 3-D holds great potential for improving our understanding of ice sheet structure and dynamics. Conducting 3-D imaging in remote areas is simplified by using lightweight and logistically straightforward sources. We report results from controlled seismic source tests carried out near the West Antarctic Ice Sheet Divide investigating the characteristics of two types of surface seismic sources, Poulter shots and detonating cord, for use in both 2-D and 3-D seismic surveys on glaciers. Both source types produced strong basal P-wave and S-wave reflections and multiples recorded in three components. The Poulter shots had a higher amplitude for low frequencies (<10 Hz) and comparable amplitude at high frequencies (>50 Hz) relative to the detonating cord. Amplitudes, frequencies, speed of source set-up, and cost all suggested Poulter shots to be the preferred surface source compared to detonating cord for future 2-D and 3-D seismic surveys on glaciers.

*Present address: Geological Sciences Building 101, University of Texas at El Paso, 500 W. University Ave., El Paso, TX 79968.

This is an Open Access article, distributed under the terms of the Creative Commons Attribution-NonCommercial-NoDerivatives licence (<http://creativecommons.org/licenses/by-nc-nd/4.0/>), which permits non-commercial re-use, distribution, and reproduction in any medium, provided the original work is unaltered and is properly cited. The written permission of Cambridge University Press must be obtained for commercial re-use or in order to create a derivative work.

27 INTRODUCTION

28 The physical and chemical properties of Antarctic glacial ice and the bed beneath it yield critical informa-
29 tion about past and present climate conditions and ice dynamics that can be used to model future scenarios
30 of ice evolution in a changing climate (Pattyn, 1996; Truffer and others, 2001; Pimentel and others, 2010;
31 Sergienko and Hulbe, 2011). Controlled-source seismic reflection profiling is a powerful method that has
32 long been used to determine ice thickness, englacial properties, as well as subglacial hydrology, lithology,
33 and topography (e.g., Bentley and Ostenso, 1961; Roethlisberger, 1972; Blankenship and others, 1987;
34 Booth and others, 2012; Picotti and others, 2015). It has also been important for determining relationships
35 between seismic velocity and density, temperature and crystal orientation fabric (COF) (e.g., Robin, 1953;
36 Bentley, 1972; Kohlen, 1974; Peters and others, 2012). The success and feasibility of controlled-source
37 seismic experiments depend, in part, on selecting seismic sources that satisfy experimental goals while also
38 being compatible with field logistical constraints. Direct comparisons of amplitudes, frequencies, and field
39 set-up procedures for different source types can help scientists select the right source for their imaging
40 project.

41 Since the 1980s, controlled sources used in Antarctica for imaging ice more than 1-km thick primarily
42 involve setting explosive charges in 15-30m deep boreholes (Blankenship and others, 1987; Luthra and
43 others, 2016). The borehole approach reduces the effects of strong seismic attenuation in the firn and
44 also reduces the ground roll (surface waves), but it requires specialized and sometimes heavy ice drilling
45 equipment, drilling expertise, and time to drill holes. Borehole shots also result in a secondary 'ghost'
46 reflection from the ice-air interface which travels closely behind the primary package of seismic waves.
47 This can complicate seismic analyses of bed properties because the bed reflection recorded at the surface
48 includes interference of the primary bed reflection and the 'ghost' reflection. Glaciologists typically reduce
49 or remove this interference of the 'ghost' with the primary bed reflection by burying shots at depths (e.g.,
50 20-25 meters) that allow for good separation (30 ms) between the primary and ghost return.

51 The problems inherent to borehole shots can be overcome using surface explosive sources, such as
52 detonating cord (Sen and others, 1998; Diez and others, 2015; Hofstede and others, 2021), shallow (< 5 m
53 depth) drilled shots, or Poulter shots. Poulter shots were originally designed and used in Antarctica for
54 seismic surveys on the Ross Ice Shelf during Byrd's second expedition from 1933-1935 and then became
55 part of standard geophysical practice (Poulter, 1950). Poulter shots involve mounting explosives above

56 the ice sheet surface with the shock wave hitting the surface generating the seismic waves. Explosions at
57 the surface or within the firn create a diving wave by compacting the firn around them. Most energy of
58 a shallow drilled explosion in firn is lost as it travels back to the surface. Surface and shallowly-drilled
59 explosions as well as other sources appear to benefit from vertical directivity of the source, one reason why
60 sources directed downward such as Poulter shots, detonating cord, and vibroseis work from the surface
61 (Poulter, 1950; Hofstede and others, 2021). For shallower (< 1 km) ice thicknesses, hammer strikes, buffalo
62 or Betsy seismic guns, and weight drop sources are also practical ice surface sources (Booth and others,
63 2013; Veitch and others, 2021). Stacking these sources can sometimes increase signal-to-noise ratios enough
64 to allow imaging of ice more than 1-km thick. On-ice vibroseis sources capable of imaging ice thicknesses
65 typically found in Antarctica are generally large and require significant logistical preparations, but the
66 seismic images can be high quality (Eisen and others, 2015).

67 In this paper, we report results from controlled seismic source tests carried out in Antarctica investigat-
68 ing the quality of two types of surface seismic sources, Poulter shots and detonating cord, for use in large
69 2-D and 3-D seismic surveys. We conducted these tests largely to identify optimal seismic sources to use for
70 3-D seismic imaging across the Eastern Shear Margin of Thwaites Glacier, as part of the Thwaites Inter-
71 disciplinary Margin Evolution (TIME) project. The field sites at Thwaites are remote locations where our
72 team will have limited cargo resources and limited field time, so we require lightweight and quick-to-setup
73 seismic sources with strong, isotropic signals and frequency content that allow imaging and characterization
74 of the ~ 2 - 2.5 km of ice and the glacier bed below.

75 We tested the surface seismic sources ~ 5 km northeast of the West Antarctica Ice Sheet (WAIS) Divide
76 Camp of the U.S. Antarctic Program, during January 2019. WAIS Divide Camp (S 79.467 °, W 112.085
77 °) is located at 1766 meters height above the WGS-84 ellipsoid and about 24 km from the ice flow divide,
78 which separates the region where the ice flows to the Ross Sea from the region where ice flows to the
79 Amundsen Sea (Conway and Rasmussen, 2009). The current ice accumulation rate is 22 cm/ year, the
80 average annual surface temperature is -30 °C, and the ice thickness is 3465 meters. The bubble close-off
81 depth at WAIS Divide is 67-77 meters (Battle and others, 2011).

82 We selected the location for the source testing to avoid noise coming from WAIS Divide Camp and
83 to align with a controlled-source seismic line that was collected during the 2008-2009 season (Horgan and
84 others, 2011). We chose to conduct our seismic sources tests in the same location to allow the possibility
85 of comparison with the drilled shots (24 meters depth) used in that survey. The profiles extended ~ 2.5 km

86 (2009) and ~ 3.25 km (2019) along-flow towards the Walgreen Coast (Amundsen Sea sector). The selected
87 testing location has the added benefit of the potential to compare the ice structure and fabric derived
88 from our seismic survey to the structure and fabric seen in the WAIS Divide ice core (Kluskiwicz and
89 others, 2017). Our seismic line is also partially co-located with a radar line collected in 2020 (Young and
90 others, 2021). Several recent studies used passive seismic data collected during the 2019 source testing
91 to investigate detailed wave propagation in firn (Chaput and others, 2022a,b, 2023) and shallow ice sheet
92 composite structure (Zhang and others, 2022).

93 This shot testing provides valuable comparisons of surface shot effectiveness for 2-D and 3-D surveys
94 of glacial environments with up to 3-km-thick ice. We tested multiple different configurations of Poulter
95 shots and multiple configurations of detonating cord to observe the signal quality, frequency content, and
96 anisotropy of seismic waves radiating from the different configurations. We also tested near-surface shots
97 with explosives placed in shallow holes, less than 5 meter depth. Poulter shot variations included type,
98 height above snow surface, and quantity of explosive. Detonating cord variations included thickness of
99 cord, amount of cord, and geometric arrangement of the cord. In this paper, we summarize the results
100 regarding the benefits and limitations of surface seismic sources in glacial environments.

101 SEISMIC SOURCE TESTING FIELD METHODS

102 The seismic tests were conducted in January 2019 along a 3.25-km-long line located ~ 5 km northeast of
103 WAIS Divide Camp and oriented along the ice flow direction, toward the Walgreen Coast (Figure 1). The
104 test shots were made at three shot points along the 3.25-km-long line (Figure 1). Shotpoint 1 (0 km offset)
105 and shotpoint 3 (3.25 km offset) were off ends of the main receiver line, and shotpoint 2 (1.625 km offset)
106 was in the middle of the receiver line. The shots were recorded on a combination of 100 Magseis Fairfield
107 Z-Land Generation 2, 5-Hz, 3-component seismic nodes (Ringler and others, 2018) and a 48-channel cabled
108 Geometrics Geode system using 4.5-Hz geophones. The recording system was configured into 3 arrays, as
109 follows: Array 1 consisted of a 2.25-km-long line of 75 nodes at 30-m spacing, with the first node at 0.5 km
110 offset and the last at 2.75-km offset; Array 2 consisted of 24 nodes in a 0.5 km radius circle, centered around
111 shotpoint 1 (0 m offset); Array 3 was a 235-meter-long line of 48 geophones at 5-m intervals between 0.265
112 km and 0.5 km offsets.

113 Nodes were buried at 30 cm depth, leveled with a bubble level, and oriented using an Antarctica-
114 weighted Brunton compass. Nodes were programmed with a sampling rate of 1000 Hz, a pre-amp gain of

115 12 dB, a linear phase Nyquist filter, and DC offset removal. The seismic nodes recorded continuously for
116 the entire experiment. The first nodes were deployed on January 6, 2019, and the nodes were retrieved
117 on January 15, 2019. Node data were merged into a PH5 volume by the Earthscope Primary Instrument
118 Center and archived at the Earthscope Data Management Center as network 2E 2018 and assembled dataset
119 18-030 (Kaip and others, 2018). The geophones remained in the same configuration during all of the shots
120 discussed in this paper. Geode data were saved in SEG2 format and converted to SEG Y for analysis. The
121 Geode cabled seismic system recorded from 1 second before the minute to 15 seconds after each minute.
122 Sources were fired on the minute using a GPS clock, a seven Joule shooting system, DaveySeis electronic
123 detonators, and a Davey Bickford Universal Seismic Interface. For safety reasons, we always use electronic
124 detonators (instead of electric detonators) to fire surface explosives. Shots were detonated on days with
125 relatively low wind and calm weather. Figure 2 contains photos and schematic diagrams of several types
126 of sources tested.

127 Twenty six surface sources were detonated at shotpoint 1, with nine different configurations of Poulter
128 shots, comprised of different amounts, heights and types of explosives (Table 1) and seventeen different
129 configurations of detonating cord shots (Table 2). The detonating cord was arranged in various patterns
130 such as lines, crosses, and swirls at the snow surface and covered with a small amount of snow to weigh
131 down the cord (Table 2). Fifteen surface sources were detonated at shotpoint 2 including four different
132 configurations of Poulter shots and eleven different configurations of detonating cord (Tables S1, S2). Nine
133 surface sources were detonated at shotpoint 3 including four different configurations of Poulter shots and
134 five different configurations of detonating cord (Tables S4, S5). At each of the three shotpoint locations,
135 we also detonated two 150-gram pentolite boosters loaded at 2.3 to 3.4 m depth in a shot hole drilled by
136 a 4-meter Kovacs ice auger (Tables 3, S3, S6). Similar shots were also made at 37 additional locations
137 along the line, with 60-m spacing, in between almost every other pair of nodes (Figure 1). These data are
138 incorporated in other papers focused on controlled-source seismic imaging (e.g., Zhang et al., in prep.).

139 For the Poulter shooting we used a custom-designed Poulter shot pole to suspend explosives at heights
140 of 1.83 to 2.44 meters (6 ft and 8 ft, respectively) above the snow surface. The pole design consisted of
141 a 6.35 by 6.35 cm square telescoping aluminum pole, that extended up to 1.52 m. A ~1 m long piece
142 of sacrificial wood (1.27 by 1.91 cm) was attached to the top, and the explosives were fastened to the
143 wood with cold-resistant tape (Figure 2) at the desired heights (either 1.83 to 2.44 meters). We detonated
144 dynamite (extra gelatin nitroglycerin dynamite, Unimax brand name), emulsion blasting agent (booster

145 sensitive emulsion, Blastex brand name), and pentolite boosters (Powerplus P brand name), with total
146 explosive weights of 2.5 kg, 4 kg, 5 kg, and 5.4 kg (Table 1). Detonating cord products included both
147 10.8 grams per meter (50 grains per foot) and 85 grams per meter (400 grain per foot) cord (Table 2).
148 Linear configurations included lines with length 16.4 m (0.18 kg) oriented inline with the receiver line and
149 perpendicular to the receiver line. Swirl configurations included swirls with length 16.4 m (diameter 3 m;
150 10.8 g/m: 0.18 kg; 85 g/m: 1.39 kg), 20.4 m (diameter 3.5 m; 10.8 g/m: 0.22 kg; 85 g/m: 1.73 kg), and 32.4
151 m (diameter 4 m; 10.8 g/m: 0.35 kg; 85 g/m: 2.75 kg). Swirls were fired inside-out (detonator in middle
152 of swirl) and outside-in (detonator on outside branch of swirl). Cross configurations included lengths of
153 8.2 m (0.09 kg), 12.2 m (0.13 kg), and 16.2 m (0.17 kg) for each branch of the cross. The crosses included
154 two linear cords with one parallel to the receiver line and one perpendicular to the receiver line.

155 As well as the source characterisation discussed in the paper, the passive seismic data recorded by
156 these arrays has allowed characterization of ambient high frequency seismic wavefields in the firn column
157 (Chaput and others, 2022a), near-surface seismic anisotropy (Chaput and others, 2022b), and estimation
158 of shear-wave velocities as well as imaging of an englacial reflector from seismic wavefield imaging (Zhang
159 and others, 2022).

160 COMPARISONS OF POULTER, DETONATING CORD, AND SHALLOW 161 DRILLED SHOTS

162 For each of the various source types, the recorded waveforms (including amplitudes, times, and frequencies)
163 were examined. Shot gathers for Poulter shot 5004 (4 kg of pentolite boosters suspended at 2.44 m above
164 the ice) recorded on array 1 and array 2 show clear P-wave, S-wave, surface wave, and air wave arrivals
165 (Figure 3). There is also a clear P-wave arrival at ~ 1.7 -1.8 seconds that we interpret as a bed reflection. A
166 multiple of the bed reflection is seen clearly at ~ 3.5 seconds (Figure S1). The air wave recorded by array
167 2 has variable travel times across the circle, most likely due to the impact of wind speed on the speed of
168 sound of the detonation (Figure 3). Shot gathers for detonating cord shot 5026 (swirl using 32.4 m of 85
169 g/m detonating cord, fired inside-out with 4m diameter, 2.75 kg explosive) recorded on array 1 and array
170 2 also show clear P-wave, S-wave, surface wave, and air wave arrivals (Figure 4). We see the same, clear
171 P-wave bed reflection at ~ 1.7 -1.8 seconds. A multiple of the bed reflection is seen clearly at ~ 3.5 seconds
172 (Figure S2, S3). The air wave recorded by array 2 is also impacted by wind speed and direction (Figure 4).
173 As expected, the vertical component contains the strongest signal, followed by the radial component, and

174 the transverse component has a less clear signal. Shot gathers for shallow drilled shot 5053, with two 150-g
175 pentolite boosters buried at 3.1 meters depth, are noisier but also show P-wave, S-wave, surface wave, and
176 air wave arrivals (Figure S4).

177 Bandwidths for Poulter and detonating cord sources were typically in the 50-150 Hz range. The
178 detonating cord shots were lower amplitude but tended to have a slightly wider bandwidth (Figure 3, 4).
179 The lower amplitude may be partially caused by the typically smaller amounts of explosive used in the
180 detonating cord sources.

181 We estimate penetration depth of the Poulter and detonating cord sources based on overall travel path
182 length observed in reflection multiples (Figure S1, S2). The penetration depth may vary based on the
183 properties of the intraglacial and subglacial layers, their impedance contrast, and quality factor, so we are
184 only able to provide rough estimates. The bed reflection multiple arrives at ~ 3.5 seconds. Assuming a
185 vertical travel path and an average velocity in ice of 3800 m/s, the total path length would be ~ 13.3 km
186 effective propagation in ice (Diez, 2014).

187 We compare the similarity of wavelets for P-waves (Figure 5) and bed reflections (Figure 6) recorded on
188 the 24 seismic nodes for all of the different types of shots detonated at shotpoint 1 (Tables 1-3). In Figures
189 5-6, the amplitudes for each shot are normalized in order to see the wavelets better. Figure S5 shows the
190 same data as Figure 5 without amplitude normalization, including Poulter shots, 5001-5009, detonating
191 cord shots, 5010 to 5026, and shallowly drilled shot 5053. Configuration details for each shot are detailed
192 in Tables 1-3. All incoming P-wave arrivals consist of a negative amplitude pulse followed by a positive
193 amplitude pulse. Waveforms are generally simple, but Poulter shots 5001, 5002, 5003, and 5004 have a
194 double positive pulse after the initial single pulse. Those sources were the Poulter shots with explosives
195 elevated at 2.44 m, so the more complex recorded wavelets may be related to the height of the explosives;
196 by contrast, Poulter shots with explosives elevated at 1.83 m appear to produce a cleaner wavelet. Plots
197 without amplitude normalization (Figure S5) clearly show that the Poulter shots have significantly higher
198 amplitudes compared to the detonating cord shots, as expected from the total explosive detonated at each
199 location (Tables 1-3). Only slight differences in wavelet and amplitude are seen for shots 5005 or 5006 (both
200 5 kg dynamite at 1.83 m) (Figure 5, S5). Shot 5007 (2.5 kg dynamite at 1.83 m) with a smaller amount
201 of explosive produces a lower amplitude P-wave, as expected (Figure S5). Shot 5008 (5 kg emulsion +
202 400g pentolite booster at 1.83 m) has a similar amplitude to shot 5006 (5 kg dynamite at 1.83 m) (Figure
203 S5). However, shot 5009 (4 kg total: 10 400 g pentolite booster at 1.83 m) has a cleaner signal and higher

204 amplitude (Figure 5, S5). For the Poulter shots, we conclude that the preferred explosive is the pentolite
205 booster, and a height of 1.83 m is preferred to 2.44 m.

206 Recordings on the circle of 24 seismic nodes of the detonating cord line parallel to the receiver line
207 (shot 5010) and the detonating cord line perpendicular to the receiver line (shot 5011) demonstrate the
208 anisotropy of the radiation pattern of waves generated by linear detonating cord shots (Figure 5, S5). The
209 detonating cord crosses (shots 5018-5020) have more isotropic wave propagation, as observed by the circle
210 of 24 nodes (Figure 5, S5).

211 Comparing detonating cord swirls with 85 g/m and various lengths and diameters of the swirls, shot
212 5021 (16.4 m of cord in a swirl with 3 m diameter) looks similar to shot 5022 (20.4 m of cord in a swirl
213 with 3.5 m diameter) and shot 5023 (32.4 m of cord in a swirl with 4 m diameter) (Figure 5, S6). The
214 larger lengths of cord and higher diameters of swirl appear to correspond to progressively lower amplitudes
215 (Figure S5, S7). This is true at all frequencies (Figure 7). Having a more tightly coiled detonating cord
216 shot seems to improve the signal generation. For the 10.8 g/m detonating cord, 5014 (32.4 m of cord in a
217 swirl with 4 m diameter) appears slightly higher amplitude than 5012 (20.4 m of cord in a swirl with 3.5
218 m diameter) and 5013 (16.4 m of cord in a swirl with 3 m diameter) (Figure S5, S7).

219 Compared to the Poulter and detonating cord shots, shot 5053, the shallowly drilled shot with two
220 0.15kg pentolite boosters installed at 3.1 meters depth, has a generally lower signal to noise ratio and a
221 more complex waveform source (Figure 5, S4, S5). Part of the reason might be the smaller amount of
222 explosive (300 g total compared to 180 g to 5.4 kg for the other sources), but the detonating cord shots
223 with a similar amount of explosive (5014, 5017, 5019, 5020) generally have cleaner signals (Figure 5) with
224 a slightly higher amplitude (Figure S5). We also observe a signal following the first arriving P-wave that
225 might be the ghost arrival from the reflected P-wave off the snow surface (Figure S4). Thus we conclude
226 that Poulter and detonating cord surface shots are preferable to shallow drilled and loaded shots.

227 Amplitude spectra for direct P, S, air, and reflected waves recorded on the 24 seismic nodes in the
228 circle for all of the different types of shots detonated at shotpoint 1 are shown in Figure 7. Configuration
229 details for each shot are detailed in Tables 1-3. Spectra clearly show that the Poulter shots (5001-5009) are
230 richer in lower frequency signals (~ 10 -20 Hz) compared to the detonating cord shots (5010-5026) and the
231 shallowly-drilled shot (5053). Detonating cord shots are richer in high frequency signals (>20 Hz) (Figure
232 7). Eighty-five g/m detonating cord produces lower frequency signals compared to the 10.8 g/m detonating
233 cord. The shallow drilled shot contains mostly higher frequency (>60 Hz) signals, with lower amplitudes

234 for frequencies <60 Hz compared to the detonating cord or the Poulter sources. Frequency content is also
235 affected by detonation velocity, which varies between sources used here.

236 Amplitude spectra for whole traces and reflected waves also show clearly that the Poulter shots are
237 stronger at low frequencies and comparable at high frequencies relative to the thicker detonating cord (85
238 g/m) (Figure 8). Thinner detonating cord (10.8 g/m) has weaker signals at all frequencies compared to
239 the Poulter shots, but the shallowly-drilled, 300 g shot is the weakest at all frequencies (Figure 7). The
240 same observations are true of the whole waves and the reflected waves (Figure 8). Whole waves include
241 time 0 to 2.05 seconds, and reflected waves include time 1.7 to 1.9 seconds. Figures 3 and 4 and S4 show
242 example shot gathers including times.

243 One of the challenges observed with all of the explosive surface sources (due to their detonation on top
244 of a relatively thick firm layer) is the generation of coherent noise (seen in Figure 3, 4, and S4). While this
245 noise may have a distinct signature in the frequency-wavenumber domain, it can be difficult to filter and
246 may require front muting. This type of noise is usually stronger for surface or shallow shots compared to
247 deeper buried shots when there is a surface firm layer. An additional challenge of the Poulter shots is that
248 they require large shot charges (5-8 times larger than the equivalent shots drilled at >20 meters). Poulter
249 shots save the weight of the hot water drill but typically require a larger weight of explosives.

250 **DIRECTIVITY OF DETONATING CORD SHOTS**

251 Shooting a detonating cord swirl inside-out versus outside-in appears to cause slight differences in the
252 wavelets recorded by the circle of nodes. In addition, the outside-in shots appear to result in a higher
253 recorded amplitude on the circle of nodes compared to the inside-out detonating cord shots (Figure S5,
254 S7). Shots 5014 and 5017 are both 32.4 m of cord arranged in a swirl with 4 m diameter, fired inside-out and
255 outside-in, respectively, and they have slightly different waveforms (Figure 5, S6) with larger amplitudes
256 for shot 5017 (Figure S5, S7). Similarly, comparing the pairs of other detonating cord shots fired inside-out
257 and outside-in shows a similar pattern (Figure 5, S5, S6, S7). The pairs of inside-out followed by outside-in
258 shots of the same length and diameter for the 85 g/m cord are: 1) 5021 and 5024 (16.4 m length and 3 m
259 diameter), 2) 5022 and 5025 (20.4 m length and 3.5 m diameter), and 3) 5023 and 5026 (32.4 m length and
260 4 m diameter) (Figure S6 and S7). The pairs of inside-out followed by outside-in shots of the same length
261 and diameter for the 10.8 g/m cord are: 1) 5012 and 5015 (16.4 m length and 3 m diameter), 2) 5013 and
262 5016 (20.4 m length and 3.5 m diameter), and 3) 5014 and 5017 (32.4 m length and 4 m diameter) (Figure

263 S6, S7). Shooting detonating cord outside-in appears to yield more high frequency energy from ~70-130 Hz
264 compared to shooting inside-out (Figure 7). Shooting outside-in also appears to result in higher amplitudes
265 for waves recorded by the circle of nodes (Figure S5, S7). We conclude that shooting outside-in produces
266 a better signal for seismic imaging (both frequency and amplitude) than shooting inside-out.

267 LOGISTICAL CONSIDERATIONS AND RECOMMENDATIONS FOR 2-D AND 268 3-D SEISMIC SURVEYS

269 The Poulter shots required less time and effort to set up compared to the detonating cord shots. For the
270 Poulter shots, the explosives and detonator were taped to the top of an approximately 1 m long piece of
271 1.27 by 1.91 cm sacrificial wood, and then the wood was connected to the top of the metal shot pole. The
272 set-up took approximately 10 minutes per shot and required little physical effort. The detonating cord had
273 to be cut from the spool to the appropriate length and then arranged in the snow. The linear arrays took
274 less time to arrange than the swirls with one person laying the detonating cord in the snow and another
275 person following behind to cover the cord with snow to weigh it down and improve coupling to the snow
276 surface. The longer 32.4 m lines took about 15 minutes to cut, lay down, wire to the detonator, and cover
277 with snow. The larger swirls of 32.4 meters took nearly 30 minutes to cut, lay down in a swirl, and cover
278 with snow, largely because the detonating cord had a tendency to curl and would not lay down flat until
279 snow weighed it down.

280 Future 2-D and 3-D seismic surveys will benefit from large numbers of seismic sources, to improve
281 the fold (number of reflection samples per bin), increase resolution of imaging, increase the azimuth of
282 recording, and increase the physical area that is imaged. The field effort and time required when wiring
283 and detonating more than 25 shots in a day was significantly more for the detonating cord swirls than for
284 the Poulter shots. However, the detonating cord linear configurations required only slightly more time per
285 shot compared to the Poulter shots. Both Poulter shots and detonating cord linear configurations can be
286 set up and detonated in 6-7 minutes, once the procedure is streamlined. Of course, drilled and loaded shots
287 require the least time to detonate once they are drilled, loaded, and wired in the ice, but significantly more
288 time and effort is expended in the drilling and loading stages. For the shallowly drilled and loaded shot
289 presented in this paper, the 3-4 meter drilled shot hole took about 20 mins to drill and load. As described
290 above, the data quality was not as good for the shallow drilled shot. A single 40 m drilled shot hole is
291 likely to take more than one hour to drill and transport the drill to the next site. Drilling to 40 m depth

292 in ice also requires specialized drilling equipment that weighs more than 500 kg. Drilling to 20-25 meters
293 depth may take as little as 20 minutes per hole, but there is also time for loading and stemming the hole
294 and for the drill set up and overnight storage time. Surface explosive sources provide a useful alternative
295 for many projects, especially imaging projects that require numerous sources, such as large 3-D surveys,
296 in remote areas or complicated terrain where time, cargo, personnel and/ or accessibility are limited. We
297 found the Poulter shots to be the best choice for optimizing the time and physical effort needed to set up
298 and detonate the shots.

299 CONCLUSIONS

300 Controlled-source shot tests near the West Antarctic Ice Sheet Divide Camp allow us to compare Poulter
301 shots (where explosives are suspended on a pole and detonated above the Earth's surface), surface deto-
302 nating cord shots, and shallowly-drilled shots at ~3 meters depth. We compare Poulter shots of various
303 sizes, explosive types, and heights above the snow surface. We compare detonating cord shots of various
304 cord weights (10.8 g/m and 85 g/m), cord lengths, cord configurations (swirl, cross, line), and detonation
305 pattern (shooting inside-out versus outside-in). We observe that Poulter shots have lower frequencies and
306 generally higher amplitudes than the detonating cord shots, perhaps because they used a larger weight
307 of explosive material. The detonating cord shots have higher amplitudes than the shallowly-drilled shot.
308 Poulter shots at 1.83 m height above snow surface resulted in a cleaner waveform compared to Poulter shots
309 at 2.44 m height above snow surface. Of the dynamite, emulsion, and pentolite booster explosive types used
310 for Poulter shots, the pentolite booster had the cleanest and strongest signal. Shooting a detonating cord
311 swirl outside-in appeared to improve both frequency and amplitude of recorded seismic signals compared
312 to shooting inside-out. We conclude from these tests that Poulter shots are a better choice than detonating
313 cord, offering signals that are richer in lower frequencies and with no compromise to high frequency content.
314 Poulter shots were also less labor intensive compared to detonating cord shots or shallowly drilled shots
315 using our work flow.

316 ACKNOWLEDGEMENTS

317 The WAIS Divide data is from the Thwaites Interdisciplinary Margin Evolution (TIME) project, a com-
318 ponent of the International Thwaites Glacier Collaboration (ITGC). Support from National Science Found-
319 ation (NSF: Grant 1739027) and Natural Environment Research Council (NERC: Grant NE/S006788/1).

320 Logistics provided by NSF-U.S. Antarctic Program and NERC-British Antarctic Survey. ITGC Contribu-
321 tion No. ITGC121.

322 The seismic instruments were provided by EarthScope Consortium through the PASSCAL Polar Sup-
323 port Services. Data collected will be available through EarthScope. The facilities of EarthScope Consor-
324 tium are supported by the National Science Foundation's Seismological Facility for the Advancement of
325 Geoscience (SAGE) Award under Cooperative Support Agreement OPP-1851037. Geodetic instruments
326 were provided by the GAGE Facility, operated by EarthScope Consortium, with support from the National
327 Science Foundation, the National Aeronautics and Space Administration, and the U.S. Geological Survey
328 under NSF Cooperative Agreement EAR-1724794.

329 We thank Leslie Blank, James King, the U.S. Air National Guard, and Kenn Borek Air for logistical
330 support. We thank Nick Gillette, Andrew Lloyd, Sridhar Anandakrishnan, Kiya Riverman, and the camp
331 staff of WAIS Divide for their field assistance and support. Finally, we are grateful for comments from
332 Coen Hofstede, an anonymous reviewer, and the editor, Bernd Kulesa, that improved the manuscript.

333 REFERENCES

- 334 Battle MO, Severinghaus JP, Sofen ED, Plotkin D, Orsi AJ, Aydin M, Montzka SA, Sowers T and Tans PP (2011)
335 Controls on the movement and composition of firn air at the west antarctic ice sheet divide. *Atmospheric Chemistry
336 and Physics*, **11**(21), 11007–11021 (doi: 10.5194/acp-11-11007-2011)
- 337 Bentley C (1972) Seismic-wave velocities in anisotropic ice: a comparison of measured and calculated values
338 in and around the deep drill hole at byrd station, antarctica. *J. Geophys. Research*, **77**, 4406–4420 (doi:
339 10.1029/JB077i023p04406)
- 340 Bentley C and Ostenso N (1961) Glacial and subglacial topography of west antarctica. *J. Glaciol.*, **3**(29), 882–911
- 341 Blankenship D, Bentley C, Rooney S and Alley R (1987) Till beneath ice stream b: 1. properties derived from seismic
342 travel times. *J. Geophys. Res.: Solid Earth*, **92**(B9), 8903–8911
- 343 Booth A, Clark R, Kulesa B, Murray T, Carter J, Doyle S and Hubbard A (2012) Thin-layer effects in glaciological
344 seismic amplitude-versus-angle (ava) analysis: implications for characterising a subglacial till unit, russell glacier,
345 west greenland. *The Cryosphere*, **6**, 909–922 (doi: 10.5194/tc-6-909-2012)
- 346 Booth AD, Mercer A, Clark R, Murray T, Jansson P and Axtell C (2013) A comparison of seismic and radar
347 methods to establish the thickness and density of glacier snow cover. *Annals of Glaciology*, **54**(64), 73–82 (doi:
348 10.3189/2013AoG64A044)

- 349 Chaput J, Aster R, Karplus M and Nakata N (2022a) Ambient high frequency seismic surface waves in the firn
350 column of central west antarctica. *J. of Glaciology*, **68**, 785–798 (doi: 10.1017/jog.2021.135)
- 351 Chaput J, Aster R, Karplus M, Nakata N, PGerstoft, Bromirski P, Nyblade A, Stephen R and Wiens D (2022b)
352 Near-surface seismic anisotropy in antarctic glacial snow and ice revealed by high frequency ambient noise. *J. of*
353 *Glaciology*, 1–17 (doi: 10.1017/jog.2022.98)
- 354 Chaput J, Aster R and Karplus M (2023) The singing firn. *Annals of Glaciology*, 1–6 (doi: 10.1017/aog.2023.34)
- 355 Conway H and Rasmussen L (2009) Recent thinning and migration of the western divide, central west antarctica.
356 *Geophys. Res. Lett.*, **36**(12), L12502
- 357 Diez A (2014) Effects of cold glacier ice crystal anisotropy on seismic data. *Ph.D. Dissertation, Alfred Wegener*
358 *Institute*
- 359 Diez A, Eisen O, Hofstede C, Lambrecht A, Mayer C, Miller H, Steinhage D, Binder T and Weikusat I (2015) Seismic
360 wave propagation in anisotropic ice - part 2: Effects of crystal anisotropy in geophysical data. *The Cryosphere*, **9**,
361 385–398 (doi: 10.5194/tc-9-385-2015)
- 362 Eisen O, Hofstede C, Diez A, Kristoffersen Y, Lambrecht A, Mayer C, Blenkner R and Hilmarsson S
363 (2015) On-ice vibroseis and snowstreamer systems for geoscientific research. *Polar Science*, **9**, 51–65 (doi:
364 10.1016/j.polar.2014.10.003)
- 365 Greene C, Gwyther D and Blankenship D (2017) Antarctic mapping tools for matlab. *Computers and Geosciences*,
366 **104**, 151–157 (doi: 10.1016/j.cageo.2016.08.003)
- 367 Hofstede C, Beyer S, Corr H, Eisen O, Hattermann T, Helm V, Neckel N, Smith EC, Steinhage D, Zeising O and
368 Humbert A (2021) Evidence for a grounding line fan at the onset of a basal channel under the ice shelf of support
369 force glacier, antarctica, revealed by reflection seismics. *The Cryosphere*, **15**(3), 1517–1535 (doi: 10.5194/tc-15-
370 1517-2021)
- 371 Horgan H, Anandakrishnan S, Alley R, Burkett P and Peters L (2011) Englacial seismic reflectivity: imaging crystal-
372 orientation fabric in west antarctica. *J. Glaciol.*, **57**(204), 639–649
- 373 Kaip G, Karplus M, Harder S, Nakata N, Booth A and Walter J (2018) West antarctic ice sheet (wais) divide source
374 testing. *International Federation of Digital Seismograph Networks*
- 375 Kluskiewicz D, Waddington E, Anandakrishnan S, Voigt D, Matsuoka K and McCarthy M (2017) Sonic methods
376 for measuring crystal orientation fabric in ice and results from west antarctic ice sheet (wais) divide. *J. Glaciol.*,
377 **63**(240), 603–617

- 378 Kohnen H (1974) The temperature dependence of seismic waves in ice. *Journal of Glaciology*, **13**, 144–147
- 379 Luthra T, Anandakrishnan S, Winberry J, Alley R and Holschuh N (2016) Basal characteristics of the main sticky
380 spot on the ice plain of Whillans ice stream, Antarctica. *Earth. Planet. Sci. Lett.*, **440**, 12–19
- 381 Morlighem M, Rignot E, Binder T, Blankenship D, Drews R, Eagles G, Eisen O, Ferraccioli F, Forseberg R, Fretwell
382 P, Goel V, Greenbaum J, Gudmundsson H, Guo J, Helm V, Hoefstede C, Howat I, Humbert A, Jokar W, Karlsson
383 N, Lee W, Matsuoka K, Millan R, Mouginot J, Paden J, Pattyn F, Roberts J, Rosier S, Ruppel A, Seroussi H,
384 Smith E, Steinhage D, Sun B, van den Broeke M, van Ommen T, van Wessem M and Young D (2020) Deep
385 glacial troughs and stabilizing ridges unveiled beneath the margins of the Antarctic ice sheet. *Nature Geoscience*,
386 **13**, 132–137 (doi: 10.1038/s41561-019-0510-8)
- 387 Pattyn F (1996) Numerical modelling of a fast-flowing outlet glacier: experiments with different basal conditions.
388 *Annals of Glaciology*, **23**, 237–246
- 389 Peters L, Anandakrishnan S, Alley R and Voigt D (2012) Seismic attenuation in glacial ice: a proxy for englacial
390 temperature. *J. Geophys. Research*, **117** (doi: 10.1029/2011JF002201)
- 391 Picotti S, Vuan A, Carcione J, Horgan H and Anandakrishnan S (2015) Anisotropy and crystalline fabric of Whillans
392 ice stream (west Antarctica) inferred from multicomponent seismic data. *Journal of Geophysical Research: Solid
393 Earth*, **120**, 4237–4262 (doi: 10.1002/2014JB011591)
- 394 Pimentel S, Flowers G and Schoof G (2010) A hydrologically coupled higher-order flow-band model of ice dynamics
395 with a Coulomb friction sliding law. *Journal of Geophysical Research*, **115** (doi: 10.1029/2009JF001621)
- 396 Poulter T (1950) The Poulter seismic method of geophysical exploration. *Geophysics*, **15**(2), 181–207
- 397 Ringler A, Anthony R, Karplus M, Holland A and Wilson D (2018) Laboratory tests of three z-land Fairfield nodal
398 5-hz, three-component sensors. *Seis. Res. Lett.*, **89**, 1601–1608 (doi: 10.1785/0220170236)
- 399 Robin G (1953) II. Summary of seismic shooting investigations in Dronning Maud Land. *Journal of Glaciology*, **2**,
400 205–211 (doi: 10.3189/S0022143000025740)
- 401 Roethlisberger H (1972) Seismic exploration in cold regions. *Science Engineering Monograph II-A2a*
- 402 Sen V, Stoffa P, Dalziel I, Blankenship D, Smith A and Anandakrishnan S (1998) Seismic surveys in central west
403 Antarctica: data and processing examples from the Anlith field tests (1994–1995). *Terra Antarctica*, **5**(4), 761–772
- 404 Sergienko O and Hulbe C (2011) 'Sticky spots' and subglacial lakes under ice streams of the Siple Coast, Antarctica.
405 *Annals of Glaciology*, **52**, 18–22

- 406 Truffer M, Echelmeyer K and Harrison W (2001) Implications of till deformation on glacier dynamics. *Journal of*
407 *Glaciology*, **47**, 123–134 (doi: 10.3189/172756501781832449)
- 408 Veitch S, Karplus M, Kaip G, Gonzalez L, Amundson J and Barthomomaus T (2021) Ice thickness estimates of
409 lemon creek glacier, from active-source seismic imaging. *Journal of Glaciology*, 1–9 (doi: 10.1017/jog.2021.32)
- 410 Young T, Martin C, Christoffersen P, Schroeder D, Tulaczyk S and Dawson E (2021) Rapid and accurate polarimetric
411 radar measurements of ice crystal fabric orientation at the western antarctic ice sheet (wais) divide ice core site.
412 *The Cryosphere*, **15**, 4117–4133 (doi: 10.5194/tc-15-4117-2021)
- 413 Zhang Z, Nakata N, Karplus M, Kaip G and Yi J (2022) Shallow ice-sheet composite structure revealed by seismic
414 imaging near the west antarctic ice sheet (wais) divide camp. *J. Geophys. Research: Earth Surface*, **127** (doi:
415 10.1029/2022JF006777)

416 TABLES

Table 1. Poulter explosive source descriptions for sources fired at shotpoint 1 as part of source testing near West Antarctic Ice Sheet (WAIS) Divide.

Shot ID	Weight (kg)	Height (m)	Type	Description
5001	5.0	2.44	dynamite	2- 75x400mm charges
5002	2.5	2.44	dynamite	1- 75x400mm charge
5003	5.4	2.44	5kg emulsion + 400g pentolite booster	2- 75x400mm charges + 400g booster
5004	4.0	2.44	10 400g pentolite booster	10 boosters taped on horizontal wood
5005	5.0	1.83	dynamite	2- 75x400mm charge
5006	5.0	1.83	dynamite	2- 75x400mm charge
5007	2.5	1.83	dynamite	1- 75x400mm charge
5008	5.4	1.83	5kg emulsion + 400g pentolite booster	2- 75x400mm charge + 400g booster
5009	4.0	1.83	10 400g pentolite booster	10 boosters taped on horizontal wood

Table 2. Detonating cord explosive source descriptions for sources fired at shotpoint 1 as part of source testing near West Antarctic Ice Sheet (WAIS) Divide.

Shot ID	Weight (kg)	Length (m)	Type	Shape	Description
5010	0.18	16.4	10.8 g/m	line	parallel to receiver line
5011	0.18	16.4	10.8 g/m	line	perpendicular to receiver line
5012	0.18	16.4	10.8 g/m	swirl	fired inside-out
5013	0.22	20.4	10.8 g/m	swirl	fired inside-out
5014	0.35	32.4	10.8 g/m	swirl	fired inside-out
5015	0.18	16.4	10.8 g/m	swirl	fired outside-in
5016	0.22	20.4	10.8 g/m	swirl	fired outside-in
5017	0.35	32.4	10.8 g/m	swirl	fired outside-in
5018	0.18	8.2	10.8 g/m	cross	2- 8.2m lengths
5019	0.26	12.2	10.8 g/m	cross	2- 12.2m lengths
5020	0.35	16.2	10.8 g/m	cross	2- 16.2m lengths
5021	1.39	16.4	85 g/m	swirl	fired inside-out
5022	1.73	20.4	85 g/m	swirl	fired inside-out
5023	2.75	32.4	85 g/m	swirl	fired inside-out
5024	1.39	16.4	85 g/m	swirl	fired outside-in
5025	1.73	20.4	85 g/m	swirl	fired outside-in
5026	2.75	32.4	85 g/m	swirl	fired outside-in

Table 3. Description of shallowly-drilled explosive source at shotpoint 1.

Shot ID	Weight (kg)	Depth (m)	Type	Description
5053	0.3	3.1	pentolite booster	2- 0.15kg booster

417 **FIGURES**

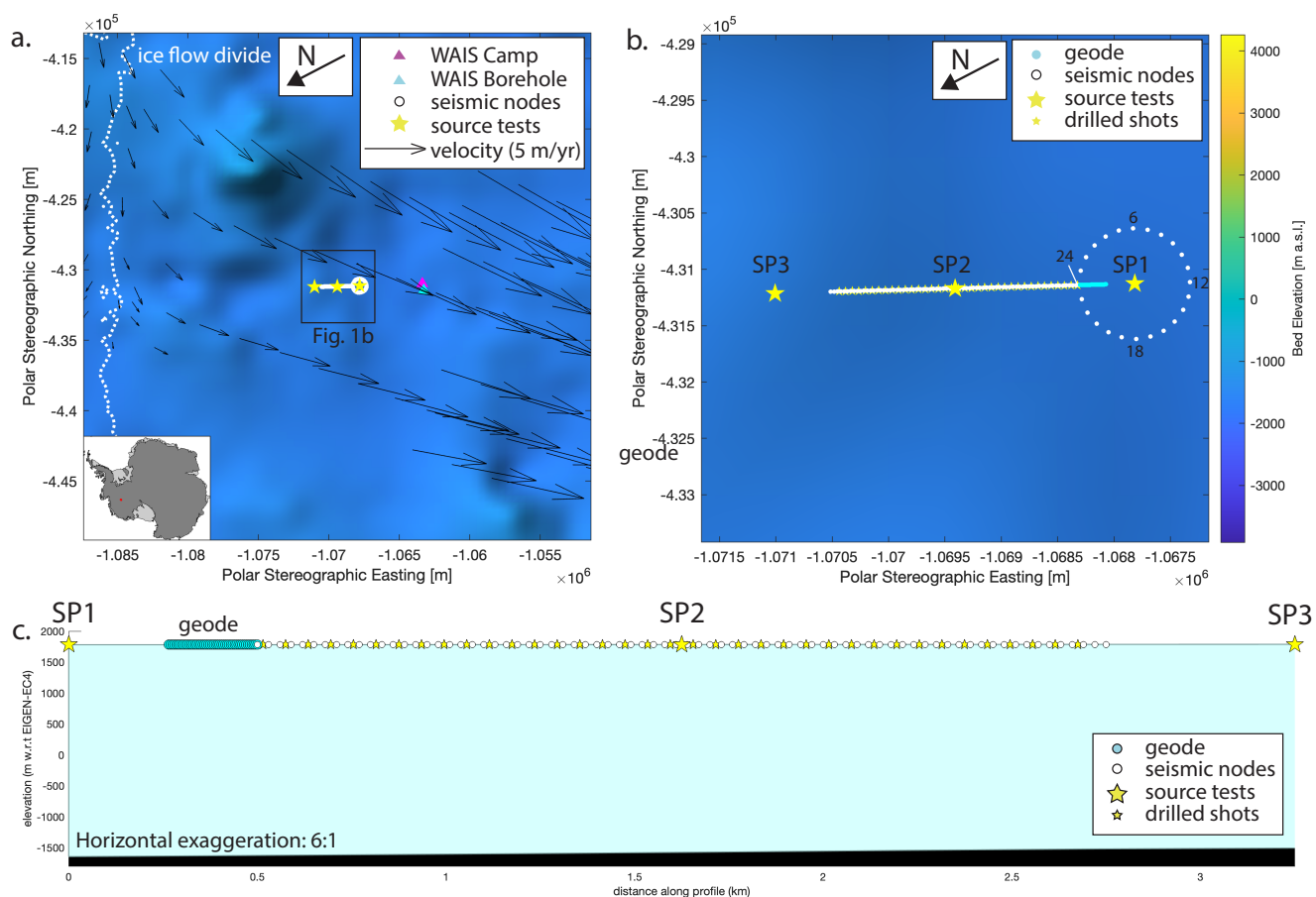


Fig. 1. Location maps for surface seismic source testing near West Antarctic Ice Sheet (WAIS) Divide. a) Map showing location of the seismic test site ~5-km northeast of WAIS Divide Camp. Bed elevation is from BedMachine v3 (Morlighem and others, 2020). Arrows show the ice flow measured near WAIS Divide (Conway and Rasmussen, 2009). Dashed white lines show the location of the ice flow divide. Ice southwest of the divide flows toward the Ross Sea, and ice northeast of the divide flows toward the Amundsen Sea. b) Zoomed in map of the seismic line and locations of sources and receivers used for shot testing. Maps were plotted in MATLAB using Antarctic Mapping Tools (Greene and others, 2017). Numbers indicate trace or node numbers for nodes in the circle. These numbers are used in Figures 3-5 for numbering the node circle traces. c) Horizontally exaggerated (6:1) cross section along the line from shotpoint (SP) 1 to 3 showing locations of sources and receivers and bed depths from BedMachine v3 (Morlighem and others, 2020).

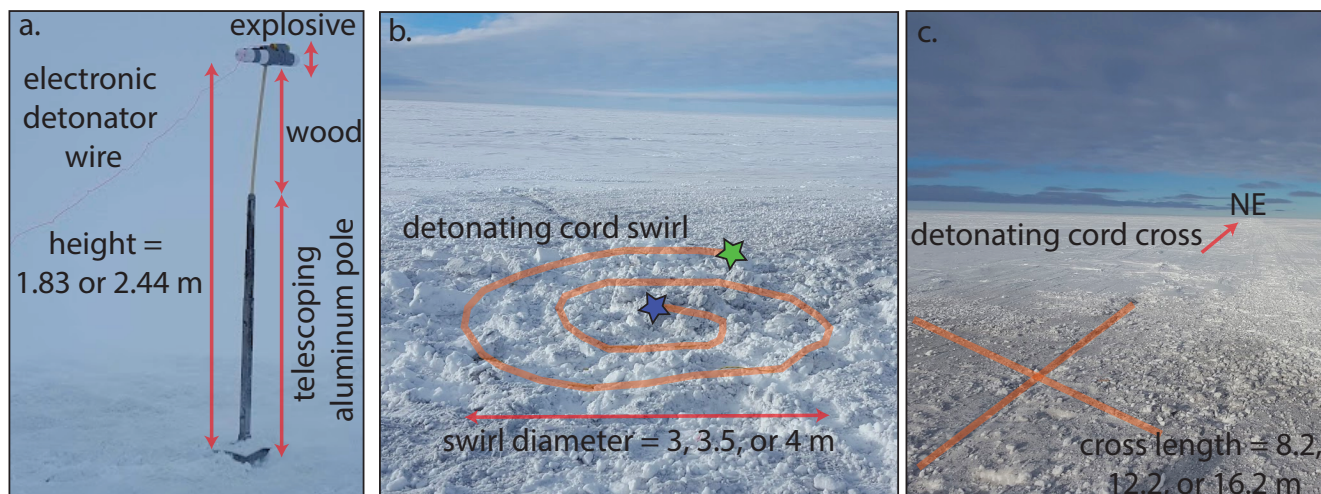


Fig. 2. Example surface source configurations tested near West Antarctic Ice Sheet Divide camp. a) Photo of an example Poulter shot, shot 5044, labelled with telescoping aluminum pole, sacrificial wood, explosive, and electronic detonator wire. Explosives included 5kg emulsion plus 400g pentolite booster detonated at 2.44 m above the snow surface. b) Photo of an example detonating cord swirl, shot 5035. The detonating cord is partially weighed down with snow, so the cord location is highlighted in orange. This swirl used 32.4 m 10.8 g/m cord with a 3 m diameter, and the swirl was fired inside-out. Green star: location of detonator for outside-in shooting; blue star: location of detonator for inside-out shooting. c. Schematic diagram of a detonating cord cross overlain on a picture of the field environment. The lines of the cross were oriented parallel (northeast) and perpendicular to the direction of the seismic line. Figures 2a, 2b, and 2c do not have the same length scales.

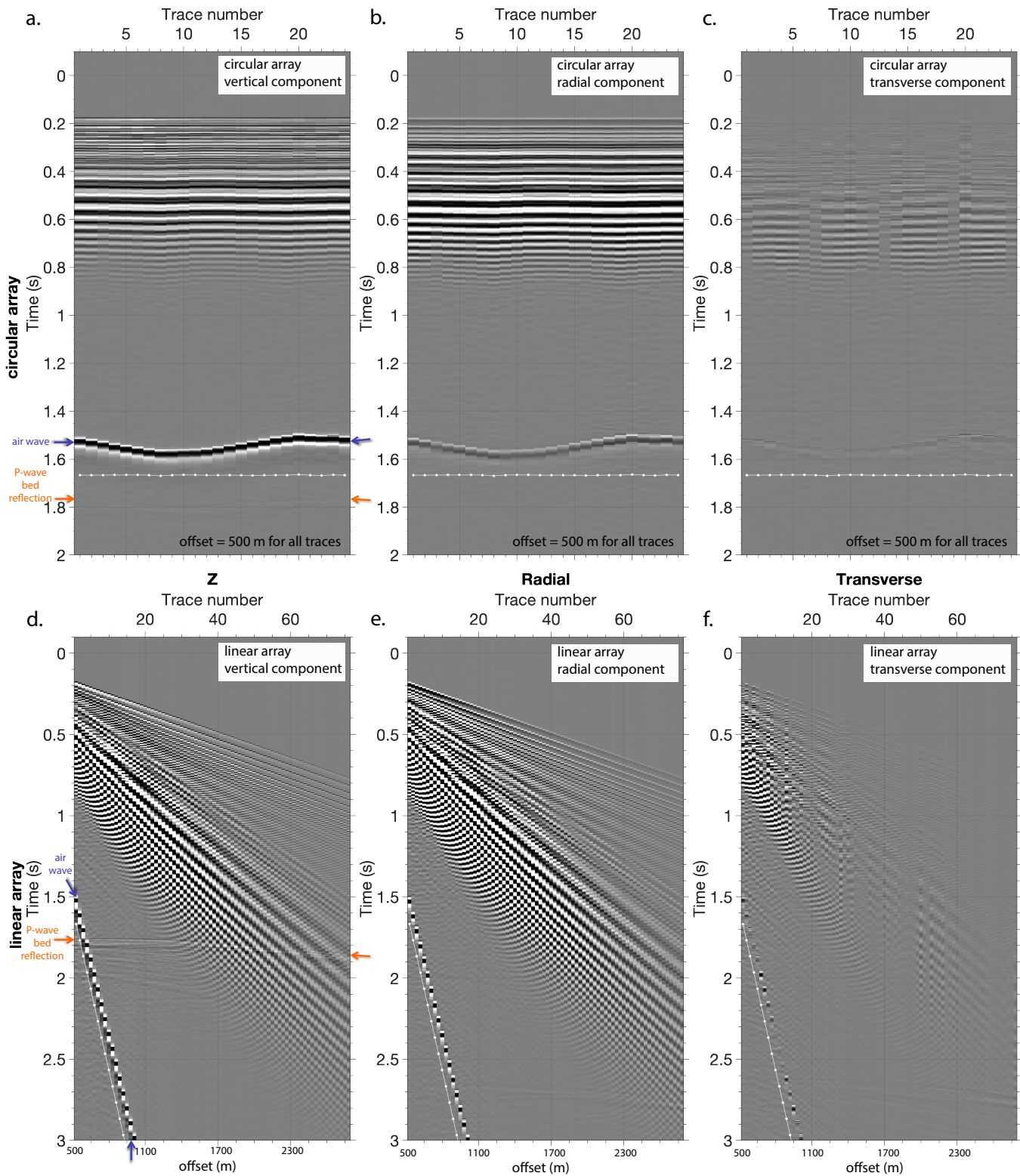


Fig. 3. Shot gather recorded in three components on array 2 (circle of 24 nodes) (a, b, c) and array 1 (line of 75 nodes) (d, e, f) for Poulter shot 5004, 10 pentolite, 400-gram boosters taped to wood, suspended at ~2.44 meters above the ice, detonated at shot point 1. DC amplitude is removed to make the mean amplitude of each shot zero. Recorded horizontal components are rotated into radial and transverse components. The white line is the theoretical air wave.

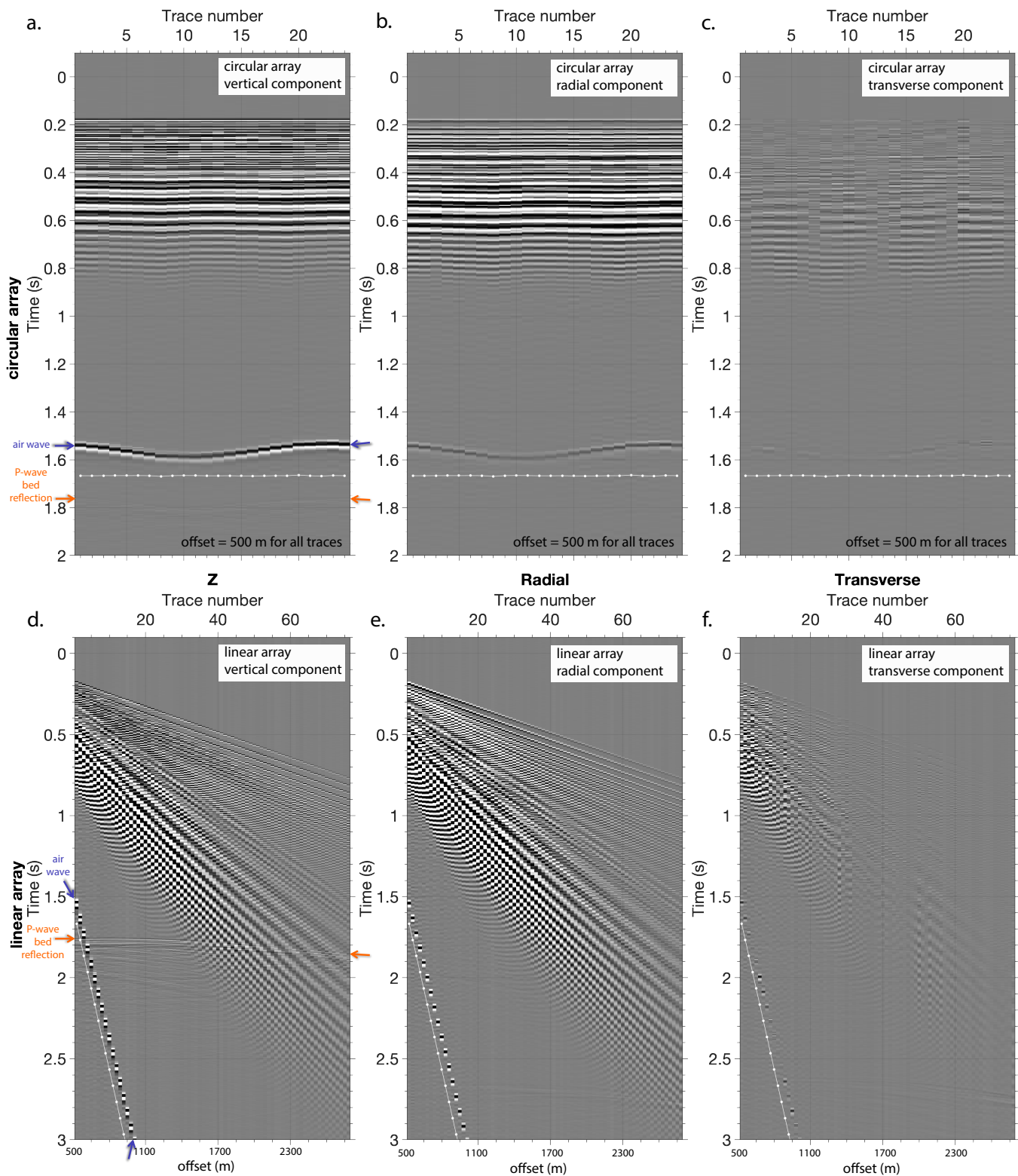


Fig. 4. Shot gather recorded in three components on array 2 (circle of 24 nodes) (a, b, c) and array 1 (line of 75 nodes) (d, e, f) for detonating cord shot 5026, a swirl using 32.4m 85 g/m fired inside-out with 4m diameter, 2.75 kg explosives, detonated at shot point 1. DC amplitude is removed to make the mean amplitude of each shot zero. Recorded horizontal components are rotated into radial and transverse components. The white line is the theoretical air wave.

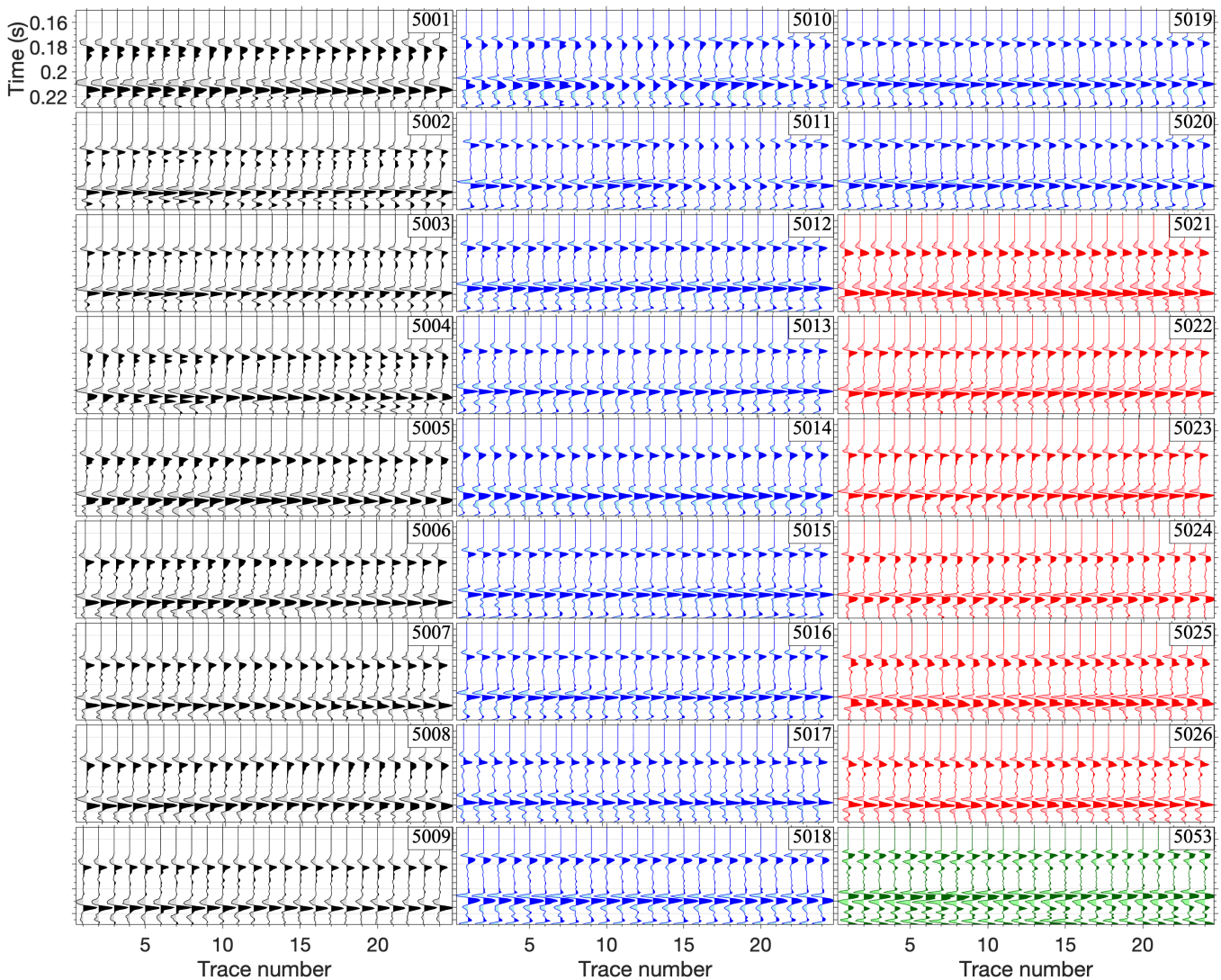


Fig. 5. Plots showing vertical component waveforms for first arriving waves recorded on the 24 seismic nodes in the circle for all of the different types of sources detonated at shotpoint 1 in order to compare wavelet similarity. Amplitudes are normalized for each shot, so amplitudes cannot be compared between different shot points. DC amplitude is removed to make the mean amplitude of each shot zero. 5001-5009 are Poulter shots. 5010 to 5020 are 10.8 g/m detonating cord shots. 5021-5026 are 85 g/m detonating cord shots. 5053 is a shallowly drilled shot. Configuration details for each shot are detailed in Tables 1-3. Figure S4 shows the same data without amplitude normalization. Waveforms for Poulter shots are colored black, for 50 grains/ft detonating cord are red, for 400 grains/ft detonating cord are blue, and for the drilled 300 g pentolite shot are colored green. For each shot, traces are ordered by seismic node number in the circle, from 1-24.

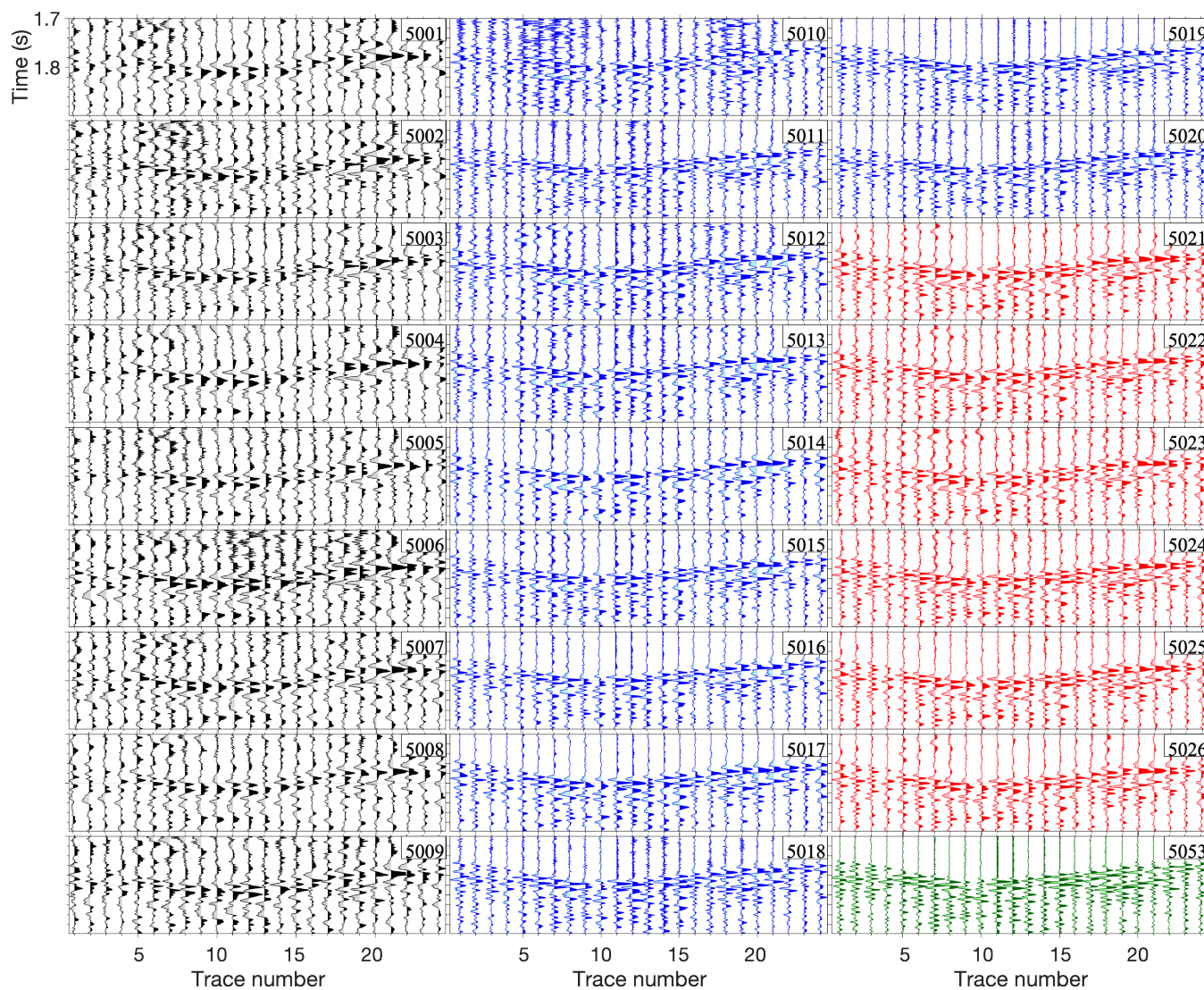


Fig. 6. Plots showing vertical component waveforms for bed reflections recorded on the 24 seismic nodes in the circle for all of the different types of sources detonated at shotpoint 1 in order to compare wavelet similarity. Amplitudes are normalized for each shot, so amplitudes cannot be compared between different shot points. DC amplitude is removed to make the mean amplitude of each shot zero. 5001-5009 are Poulter shots. 5010 to 5020 are 10.8 g/m detonating cord shots. 5021-5026 are 85 g/m detonating cord shots. 5053 is a shallowly drilled shot. Configuration details for each shot are detailed in Tables 1-3. Waveforms for Poulter shots are colored black, for 50 grains/ ft detonating cord are red, for 400 grains/ ft detonating cord are blue, and for the drilled 300 g pentolite shot are colored green. For each shot, traces are ordered by seismic node number in the circle, from 1-24.

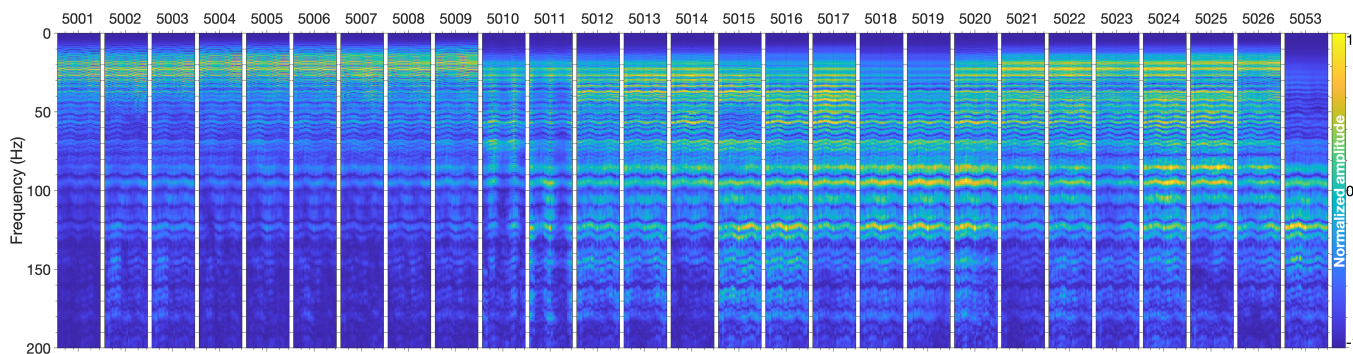


Fig. 7. Amplitude spectra showing amplitude for each frequency for a time window including the direct P, S, air, and reflected waves (time 0 to 2.05 seconds, as shown in Figures 3 and 4) recorded on the vertical component of the 24 seismic nodes in the circle for all of the different types of shots detonated at shotpoint 1. Amplitude is normalized for each shot. 5001-5009 are Poulter shots. 5010 to 5026 are detonating cord shots. 5053 is a shallowly drilled shot. Configuration details for each shot are detailed in Tables 1-3.

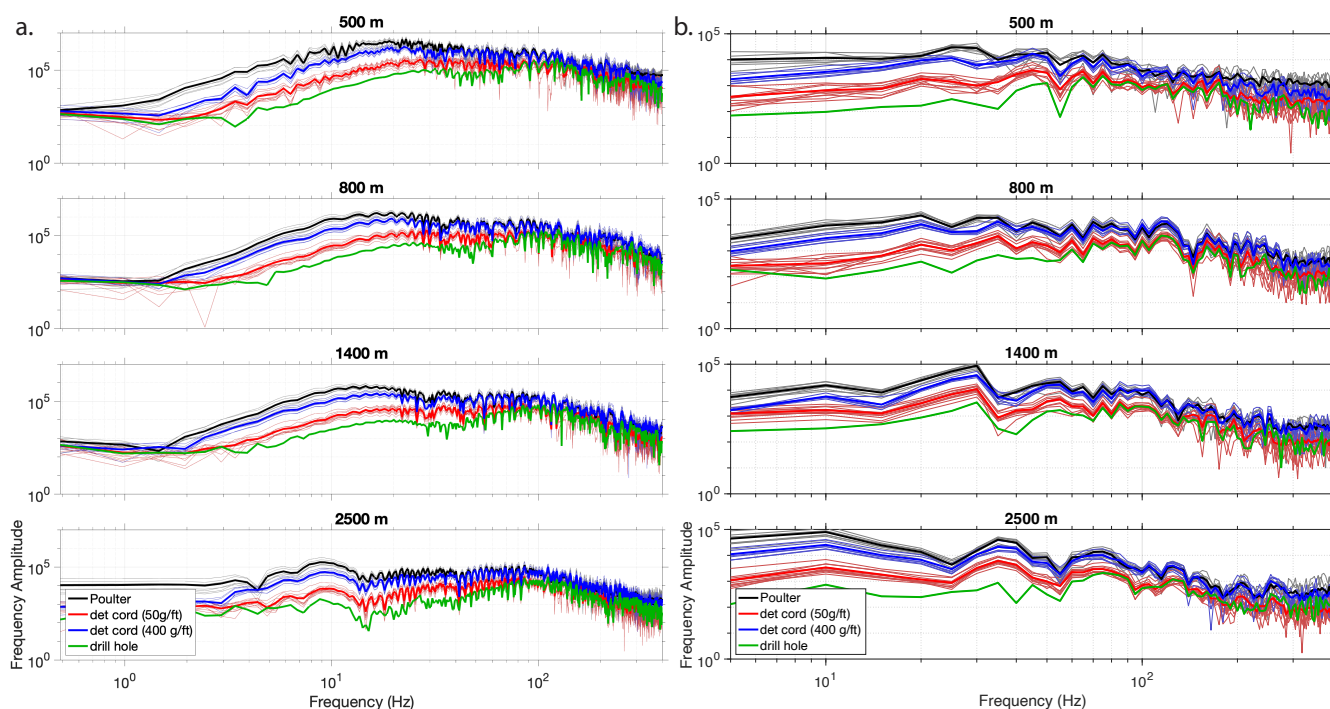


Fig. 8. Comparison of amplitude spectra for a) the whole traces (time 0 to 2.05 seconds) and b) the reflected waves (time 1.7 to 1.9 seconds). Example shot gathers showing times are shown in Figures 3-4. Colors indicate different shot types: Poulter (black), detonating cord (50 grains/ ft; red), detonating cord (400 grains/ ft; blue), drilled shot (green). The Poulter shots are stronger for low frequencies and comparable at high frequencies relative to the thicker detonating cord. The thinner detonating cord is less strong at all frequencies, and the shallowly-drilled, 300 g shot is the weakest at all frequencies. Bold lines are the average frequency amplitude for each shot type.